

# Solvent-Driven Room-Temperature Synthesis of Nanoparticles $\text{BiPO}_4\text{:Eu}^{3+}$

Chaochao Fu,<sup>†</sup> Guangshe Li,<sup>‡</sup> Minglei Zhao,<sup>†</sup> Liusai Yang,<sup>†</sup> Jing Zheng,<sup>†</sup> and Liping Li<sup>\*†</sup>

<sup>†</sup>Key Lab of Optoelectronic Materials Chemistry and Physics, Fujian Institute of Research on the Structure of Matter, Graduate School of Chinese Academy of Sciences, Fuzhou 350002, People's Republic of China

<sup>‡</sup>State Key Lab of Structural Chemistry, Fujian Institute of Research on the Structure of Matter, Graduate School of Chinese Academy of Sciences, Fuzhou 350002, People's Republic of China

**ABSTRACT:** In this work, a novel solvent-driven room-temperature synthesis of  $\text{BiPO}_4\text{:Eu}^{3+}$  nanoparticles was presented. By virtue of 11 solvents with different properties and function groups, phase structure and composition of  $\text{BiPO}_4\text{:Eu}^{3+}$  can be systematically tailored. Hexagonal phase (HP) of  $\text{BiPO}_4\text{:Eu}^{3+}$  was obtained in water and hydrophobic organic solvents such as arenes and cyclohexane, while low-temperature monoclinic phase (LTMP) was prepared in hydrophilic alcohols. In other solvents (i.e., hydrophilic ethers, aldehydes, ketones, and carboxylic acids), a mixture of HP and LTMP was formed, in which the relative content of LTMP gradually increased following the above solvent sequence. It is also found that particle sizes of  $\text{BiPO}_4\text{:Eu}^{3+}$  nanoparticles were closely related to the phase structure: HP exhibited a comparatively larger particle size. The phase evolution processes for both polymorphs with varying solvents were investigated in details. Photoluminescence (PL) properties were sensitive to the phase structure and compositions of the final products. With increasing the phase content of LTMP, the lifetimes and quantum yields both increased. The methodology reported here is fundamentally important, which may give a novel insight into the polymorph-controlled synthesis for further optimized materials performance.

## 1. INTRODUCTION

Crystal polymorphism, which embodies the ability of molecules to form diverse packing arrangements displaying different physical and chemical characteristics, is of paramount importance in many fields such as pharmacology, solid-state chemistry, and material science.<sup>1</sup> Now, synthesis of nanomaterials with controlled polymorphs is of fundamental and technological interest, since it is possible to tune their polymorph-dependent physical and chemical properties for potential applications.<sup>2,3</sup> However, it still faces a great challenge in preparing polymorphs, because of their unstable properties under atmosphere conditions. Over the past decades, many great efforts have been devoted to solution-based chemical routes, such as sol-gel, precipitation, solvothermal/hydrothermal, and template synthesis with an aim to stabilize some polymorphs. It is well-established that reaction parameters, such as temperature, time, and pH value play the important roles in controlling the phase structure, morphology, and size. Solvent is an essential part of the chemical routes, while its effect is usually neglected for preparing the polymorphs. For example, depending on the solvents, some metastable phases can be stabilized by lattice water.<sup>4</sup> One may expect that polymorph-tailoring of nanomaterials could be highly possible if the chemical properties (i.e., function group effects, electronegativity, polarity) of solvents can be understood for different polymorphs.

It is well-known that bismuth phosphate ( $\text{BiPO}_4$ ) has three different modifications such as hexagonal phase (HP), low-temperature monoclinic phase (LTMP), and high-temperature monoclinic phase (HTMP),<sup>4,5</sup> which enables extensive applications such as catalytic reactions,<sup>4,6</sup> orthophosphate-ion sensors,<sup>7</sup> separating radioactive elements,<sup>8</sup> and photocatalysis.<sup>9</sup>

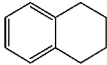
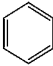
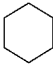
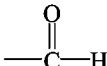
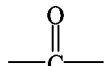
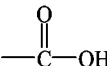
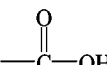
Moreover, because of the structural similarities to lanthanide orthophosphate ( $\text{LnPO}_4$ ), which was electron energy level matching rare-earth elements,  $\text{BiPO}_4$  is a promising host material of rare-earth ions for creating many distinct properties. For example, Xu et al. have reported the photoluminescence of  $\text{BiPO}_4\text{:Ln}$  ( $\text{Ln} = \text{Eu}, \text{Tb}, \text{Dy}$ ) with LTMP, which was synthesized using the hydrothermal method at 100 °C.<sup>10</sup> Zhao and Li et al. investigated the luminescence of all polymorphs of  $\text{BiPO}_4\text{:Eu}^{3+}$  and found that HP can be prepared in water at room temperature, while LTMP was obtained by calcining HP at 500 °C.<sup>5</sup> Up to now, many methods such as hydrothermal, microwave heating, and solid state reactions were used to synthesize  $\text{BiPO}_4$ , while these syntheses usually have to be performed under severe conditions of high-temperatures.<sup>11</sup> These restrictions may also limit the potential applications of nanomaterials. Therefore, low-temperature synthesis, especially room-temperature growth of nanocrystals, provides several attractive advantages. Unfortunately, room-temperature synthesis is still extremely challenging.

In this work,  $\text{Eu}^{3+}$ -doped  $\text{BiPO}_4$  with two different polymorphs were prepared through modulating solvents at room temperature. The possible formation mechanisms in different solvents were discussed schematically. The corresponding luminescence properties with phase evolutions were also investigated. These methodologies may pave a general route for preparing other polymorphs by considering the solvent effect with optimized materials performance.

Received: February 29, 2012

Published: May 3, 2012

Table 1. Sample Names, Functional Groups of Solvents, Relative Weight Losses Determined by TGA ( $\Delta m/m_0$ ), Eu Content from ICP Analysis, and Experimental Molecular Formula<sup>a</sup>

Samples	Solvents	Functional groups	$\Delta m/m_0$ from TGA (%)	Eu content (wt%)	Molecular formula
S1	H <sub>2</sub> O	-	2.8	2.13(4)	Bi <sub>0.956</sub> Eu <sub>0.044</sub> PO <sub>4</sub> ·0.482H <sub>2</sub> O
S2	Tetranap		4.1	1.52(3)	Bi <sub>0.968</sub> Eu <sub>0.032</sub> PO <sub>4</sub> ·0.718H <sub>2</sub> O
S3	Benzene		4.5	1.45(3)	Bi <sub>0.969</sub> Eu <sub>0.031</sub> PO <sub>4</sub> ·0.791H <sub>2</sub> O
S4	Cyclohexane		3.8	1.53(3)	Bi <sub>0.968</sub> Eu <sub>0.032</sub> PO <sub>4</sub> ·0.663H <sub>2</sub> O
S5	-	-	4.1	2.09(4)	Bi <sub>0.956</sub> Eu <sub>0.044</sub> PO <sub>4</sub> ·0.716H <sub>2</sub> O
S6	Diethylene glycol dimethyl ether	—C—O—C—	3.9	0.52(1)	Bi <sub>0.989</sub> Eu <sub>0.011</sub> PO <sub>4</sub> ·0.684H <sub>2</sub> O
S7	Caprylaldehide		4.6	2.43(5)	Bi <sub>0.964</sub> Eu <sub>0.036</sub> PO <sub>4</sub> ·0.808H <sub>2</sub> O
S8	Acetone		3.2	1.75(4)	Bi <sub>0.964</sub> Eu <sub>0.036</sub> PO <sub>4</sub> ·0.554H <sub>2</sub> O
S9	Propionic acid		3.4	2.16(4)	Bi <sub>0.955</sub> Eu <sub>0.045</sub> PO <sub>4</sub> ·0.589H <sub>2</sub> O
S10	Methanoic acid		2.2	2.29(5)	Bi <sub>0.953</sub> Eu <sub>0.047</sub> PO <sub>4</sub> ·0.377H <sub>2</sub> O
S11	Ethylene glycol methyl ether	—OH	1.2	2.18(4)	Bi <sub>0.956</sub> Eu <sub>0.044</sub> PO <sub>4</sub> ·0.203H <sub>2</sub> O
S12	Ethylene glycol	—OH	1.0	0.32(1)	Bi <sub>0.993</sub> Eu <sub>0.007</sub> PO <sub>4</sub> ·0.170H <sub>2</sub> O

<sup>a</sup>S5 is the sample prepared by directly milling the starting materials in air.

## 2. EXPERIMENTAL SECTION

**2.1. Materials.** Bi(NO<sub>3</sub>)<sub>3</sub>·5H<sub>2</sub>O, Eu(NO<sub>3</sub>)<sub>3</sub>·6H<sub>2</sub>O, and NH<sub>4</sub>H<sub>2</sub>PO<sub>4</sub> were used as starting materials. Deionized water, tetranap, benzene, cyclohexane, diethylene glycol dimethyl ether, caprylaldehide, acetone, propionic acid, methanoic acid, ethylene glycol methyl ether, and ethylene glycol were chosen as the solvents to prepare BiPO<sub>4</sub>:Eu<sup>3+</sup> nanocrystals. All chemicals were analytical-grade reagents and used directly without further purification.

**2.2. Preparation of Polymorphic BiPO<sub>4</sub>:Eu<sup>3+</sup>.** Eu<sup>3+</sup>-doped BiPO<sub>4</sub> nanoparticles were prepared via a simple precipitation method at room temperature. The preparation procedure can be briefly described as follows: 1.9 mmol Bi(NO<sub>3</sub>)<sub>3</sub>·5H<sub>2</sub>O and 0.1 mmol Eu(NO<sub>3</sub>)<sub>3</sub>·6H<sub>2</sub>O were added into 80 mL of a benzene solution under magnetic stirring to form a homogeneous suspension. Soon afterward, 0.2 mmol NH<sub>4</sub>H<sub>2</sub>PO<sub>4</sub> was put into the solution. The solution was then allowed to remain in air at room temperature for 4 h. The resulting precipitates were centrifuged and sufficiently washed with absolute ethanol and deionized water. Eventually, the samples were dried at 60 °C in air for 5 h and milled to fine powders for further characterization. The sample was marked as S3 and other BiPO<sub>4</sub> samples were also synthesized under identical conditions, using different solvents, which are listed in Table 1.

**2.3. Characterization.** Phase structures of the samples were characterized by powder X-ray diffraction (XRD) on a Rigaku Miniflex apparatus (Cu K $\alpha$ ,  $\lambda$  = 0.15418 nm). Lattice parameters and the relative contents of hexagonal and monoclinic phases were calculated

by Rietveld refinement using GSAS software. Nickel powder serves as an internal standard for peak position determination. Particle sizes and morphologies of the samples were observed by field-emission scanning electron microscopy (SEM) (JEOL, Model JSM-6700) and transmission electron microscopy (TEM) (JEOL, Model JEM-2010). Eu contents in the samples were quantitatively determined using inductive coupled plasma–optical emission spectroscopy (ICP-OES). Thermogravimetric analysis (TGA) was conducted on a Netzsch Model STA449F3 thermal analyzer at a heating rate of 20 K min<sup>-1</sup> in air from room temperature to 1100 °C. Infrared spectra of the samples were measured on a Perkin–Elmer IR spectrophotometer, using a KBr pellet technique.

Photoluminescence (PL) properties and lifetime curves of the samples were obtained on a Varian Cary Eclipse Fluorescence spectrometer. All measurements were gained under the same conditions (such as mass, light path, and so on).

## 3. RESULTS

**3.1. Phase Tailoring of BiPO<sub>4</sub>:Eu<sup>3+</sup> via Solvent-Driven Synthesis.** Eu<sup>3+</sup>-doped hexagonal phase (HP) and low-temperature monoclinic phase (LTMP) of BiPO<sub>4</sub> were synthesized in different solvents using a facile precipitation method at room temperature. Phase purity and structure of all samples were confirmed by XRD patterns. As shown in Figure 1, the XRD pattern of sample S1 prepared in water was well-

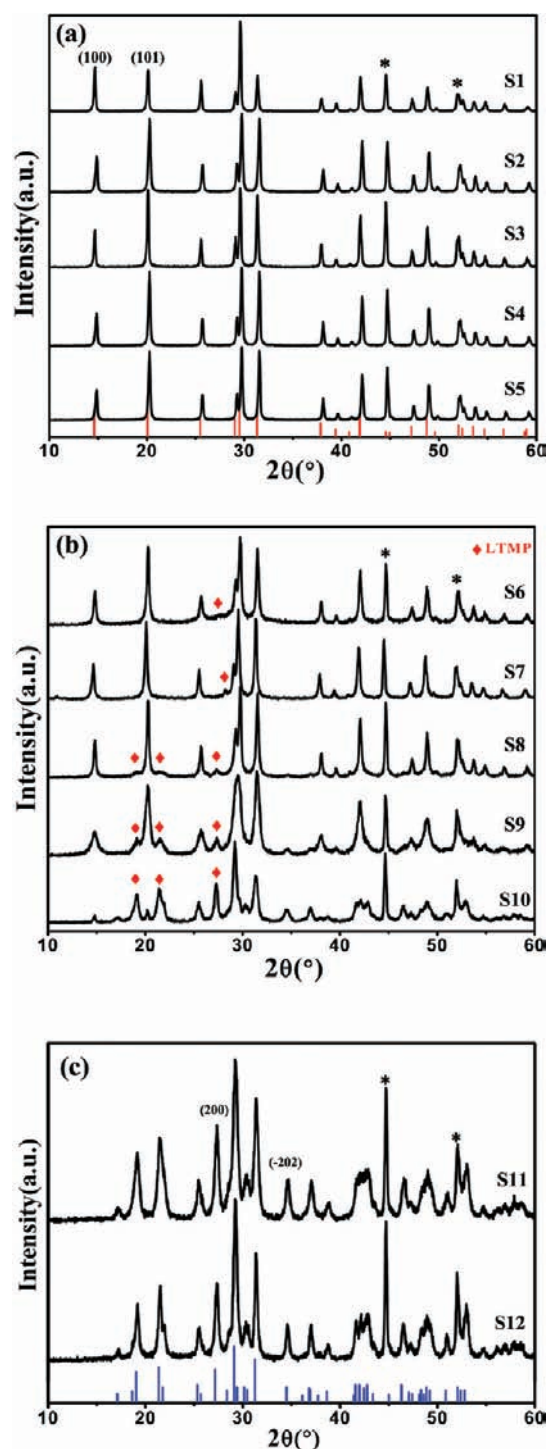


**Figure 1.** X-ray diffraction (XRD) patterns of the samples: (a) S1–S5, in a single phase of hexagonal structure, (b) S6–S10, in a mixed phase of hexagonal phase (HP) and low-temperature monoclinic phase (LTMP), and (c) S11 and S12, in a pure LTMP structure. Vertical bars represent the standard diffraction data for HP and LTMP, respectively. The black asterisk symbol denotes the internal standard nickel.

indexed, according to the standard diffraction data for HP (JCPDS, File Card No. 15-0766) and no other peaks were observed, which indicated the formation of pure HP. This result is compatible with the experimental result of Zhao and Li et al.<sup>5</sup> The samples (S2, S3, and S4) prepared in solvents of tetra-nap, benzene, and cyclohexane, respectively, exhibited the same

XRD pattern as sample S1, which also confirms their crystallization in a pure HP structure. For samples S6 and S7, which were obtained in diethylene glycol dimethyl ether and caprylaldehyde, respectively, however, several weak diffractions, such as those at  $2\theta = 27.4^\circ$  and  $28.1^\circ$  were observed. Data analysis showed that these peaks could be assigned to (200) and (002) diffractions of LTMP. With regard to sample S8, which was prepared in acetone, more diffractions from LTMP, such as lines (011) and  $(\bar{1}11)$  were clearly seen. Moreover, when the samples were precipitated in propionic acid and methanoic acid, the diffraction peaks of LTMP became extremely strong and the intensity of diffractions of HP decreased. These results demonstrate that samples S6–S10 are all a mixed phase of HP and LTMP. Unlike samples S1–S10, sample S11 and S12, which were obtained in ethylene glycol methyl ether and ethylene glycol, respectively, did not show any HP diffractions. The diffraction patterns of samples S11 and S12 matched the standard data for LTMP well (JCPDS File Card No. 15-0767), which indicates the formation of a single LTMP phase for samples S11 and S12. Therefore, it can be concluded that both HP and LTMP of  $\text{BiPO}_4$  could be readily prepared by choosing the suitable solvents.

Phase contents and lattice volume of components HP and LTMP for all samples were obtained by structural refinements. As indicated in Table 2, among the four samples with pure HP (samples S1–S4), sample S1, which was prepared in  $\text{H}_2\text{O}$ , exhibited the largest volume, while the other samples have almost the same volume. For samples that crystallized in a pure LTMP structure (samples S11 and S12), the lattice volume for sample S11 is smaller than that for sample S12. Surprisingly, from sample S6 to sample S10, the phase content of HP exhibited a continuous decrease (e.g., from 95.2% for sample S6 to 10% for sample S10). Thus, it can be seen that phase-tailoring can be realized by varying the solvents. Meanwhile, the lattice parameters (not shown) also exhibited a different variation.

From Figure 1, it can also be seen that the diffraction peaks of monoclinic phase are broader than those of hexagonal phase, which indicates that  $\text{BiPO}_4$  with a monoclinic phase prepared at room temperature exhibited a fine particle size. The particle sizes for HP and LTMP were estimated using the Scherrer formula,

$$D = \frac{0.9\lambda}{\beta \cos \theta}$$

where  $\lambda$  is the X-ray wavelength employed ( $\lambda = 1.5418 \text{ \AA}$ ),  $\theta$  the diffraction angle of the given peak, and  $\beta$  the half-width after subtracting the instrumental broadening. The calculations were carried out using two diffraction peaks for each phase, i.e., (100) and (101) peaks for HP, and (200) and  $(\bar{2}02)$  peaks for LTMP, since all these peaks are not overlapped with others. As listed in Table 2, the particle size for sample S1 estimated using the (101) diffraction was  $\sim 90 \text{ nm}$ , whereas the half-width of diffraction (100) was extremely narrow, indicating a large particle size. Therefore, it can be expected that sample S1 does not have a spherical morphology. Sample S2 exhibited slightly broadened diffraction peaks. The particle sizes for sample S2 (estimated) are  $\sim 60 \text{ nm}$  for both diffraction peaks, showing an almost-spherical morphology. Instead, sample S3 had a particle size that was too large to be estimated using the Scherrer formula. Compared with samples in a single HP phase, the samples in mixed phases showed a relatively small particle size. The particle sizes of HP phase for samples S6, S7, S8, and S10

Table 2. Sample Names, Particle Sizes, Phase Contents, and Lattice Volume for All Samples

samples	Particle Size (nm)				Phase content (mol %)		Lattice Volume ( $\text{\AA}^3$ )	
	HP <sub>(100)</sub>	HP <sub>(101)</sub>	LTMP <sub>(200)</sub>	LTMP <sub>(-202)</sub>	HP	LTMP	HP	LTMP
S1	>100	90			100	0	273.75(2)	
S2	56	63			100	0	272.55(1)	
S3	>100	>100			100	0	272.50(2)	
S4	71	91			100	0	272.00(2)	
S5	70	91			100	0	269.77(3)	
S6	35	39			95.2	4.8	274.09(3)	302.0(9)
S7	38	41			91.6	8.4	274.36(2)	278.0(4)
S8	45	45	23	10	69.6	30.4	271.09(1)	294.1(3)
S9	11	16	13	12	58.9	41.1	269.24(8)	306.3(2)
S10	41	42	23	13	10.0	90.0	272.5(2)	295.6(1)
S11			18	18	0	100		294.71(3)
S12			22	28	0	100		295.79(8)

were distributed in the range of 35–45 nm, while the particle size for sample S9 is only 16 nm, as estimated from peak (101). From Table 2, it can be found that the particle sizes of LTMP are smaller than that of HP for either single-phase samples or mixed-phase samples. The largest size estimated for sample S12 is  $\sim 28$  nm, which is much smaller than that for samples S1–S4, and even smaller than that of the sample S5, which was prepared by room-temperature grinding. This result demonstrates that BiPO<sub>4</sub> with a pure HP is easily formed and steadily grown at room temperature, if water molecules are involved in the reaction system.

Particle sizes and morphologies for all BiPO<sub>4</sub>:Eu<sup>3+</sup> nanocrystals were further investigated by SEM and TEM. Typical SEM images of the samples prepared in different solvents are exhibited in Figure 2. It can be seen that sample S1 shows a rod-like morphology with several hundred nanometers in length and  $\sim 100$  nm in diameter. Sample S3 is mainly constructed by aggregated polyhedrons in the range of 350–450 nm, while sample S4 exhibited an ellipsoid-like shape with dimensions of several hundred nanometers. These observations demonstrate that samples in a single HP phase have large particle sizes, which is consistent with the XRD analysis, as described above. For the samples in a mixed phase of HP and LTMP, samples S6 and S7 consisted of spherical particles, while sample S8 showed a mixture of spherical and rod-like particles. Sample S10 exhibited a spindle-like architecture, as constructed by a self-assembly of tiny primary particles 20–30 nm in dimension. Different from the samples in the HP phase, sample S12 was agglomerated by extremely small particles.

All samples were further examined by TEM. Figures 3a and 3d show the TEM images of typical samples S3 and S12, respectively. HRTEM images in Figures 3b and 3e for samples S3 and S12 depict the well-resolved lattice fringes, which indicates a single-crystal nature. The distance between two neighboring fringes in Figure 3b is 0.610 nm, which is compatible with that of the (100) plane for HP, while in Figure 3e the lattice spacing is 0.308 nm, corresponding to the (120) plane of LTMP. The particle size distributions were gained through a statistical evaluation of 40–60 grains in TEM pictures and fitted by a Logistic peak function,<sup>12</sup> as shown in Figures 3c and 3f. The average particle sizes were 103 and 54 nm for samples S3 and S12, respectively, as synthesized in benzene and ethylene glycol, respectively. The particle size distribution of sample S12 is relatively homogeneous when comparing to sample S3. TEM images for samples S2, S5, S9, and S11 were also comparatively studied. As shown in Figure 3,

the average particle sizes for samples S2, S3, and S5 in HP were  $\sim 100$  nm, which are apparently bigger than those of samples S11 and S12 in LTMP.

Phase structures of all samples were verified by IR spectra. Figure 4 compares the IR spectra of the selected samples S1, S8, S10, and S11. For sample S1 in pure HP, vibrations in the range of 400–4000 cm<sup>-1</sup> can be clearly separated into the contributions from P–O and O–H bonds. The very intense band centered at 1023 cm<sup>-1</sup> is ascribed to the  $\nu_3$  stretching vibration of PO<sub>4</sub> groups,<sup>4</sup> and the sharp bands at 599 and 538 cm<sup>-1</sup> correspond to the vibrations  $\delta(\text{O–P–O})$  and  $\nu_4(\text{PO}_4)$ , respectively.<sup>4,13,14</sup> The strong band centered at 3485 cm<sup>-1</sup> characterizes the stretching vibration,  $\nu(\text{O–H})$  of the water molecules that are coordinated directly to Bi atoms, while the shoulder at 3550 cm<sup>-1</sup> is due to the stretching vibration of  $\nu(\text{O–H})$  for water molecules adsorbed on sample surface.<sup>15,16</sup> The band at 1603 cm<sup>-1</sup> is due to the bending vibration,  $\delta(\text{H–O–H})$  of water molecules.<sup>16,17</sup> For sample S11 in a pure LTMP phase, besides the bands of  $\nu(\text{O–H})$  and  $\delta(\text{H–O–H})$  of adsorbed water molecules, seven vibrations were observed at wavenumbers below 1300 cm<sup>-1</sup>. These bands are characteristic of the vibrations of P–O bonds in a monazite structure of C<sub>1</sub> symmetry.<sup>4</sup> According to the group theory, four bands at 1083, 1002, 956, and 925 cm<sup>-1</sup> are assigned to the  $\nu_3$  vibrations of P–O bond that result from the distortion of tetrahedral phosphate groups. Three bands appeared at 616, 551, and 528 cm<sup>-1</sup> are attributed to the vibrations of PO<sub>4</sub> groups, characteristic of the phosphate groups in a monoclinic structure. For samples S8 and S10 in mixed phase P–O vibration bands were similar to those of pure phase samples S8 and S1, respectively, while these vibration bands were obviously broadened when comparing to pure-phase samples. It should be mentioned that the band observed at 1387 cm<sup>-1</sup> for S8, S10, and S11, and that at 1552 cm<sup>-1</sup> for sample S10 are attributed to the vibration of CO<sub>2</sub> adsorbed on the sample surface.<sup>17,18</sup> The presence of the vibration of CO<sub>2</sub> also confirms the small particle sizes for samples S8, S10, and S11. In addition, the peaks at 2925 and 2843 cm<sup>-1</sup> were possibly originated from the vibration of methanoic acid molecules adsorbed on sample surface of S10. The adsorption of methanoic acid molecules on sample surface also results in a lightly pink sample color.

Depending on the phase compositions, water contents for all samples could be different. The relative water contents were investigated by TGA. As indicated in Figure 5a, for a typical sample S3, a continuous mass loss with a total amount of 4.5 wt % was observed to occur from room-temperature to 580 °C.

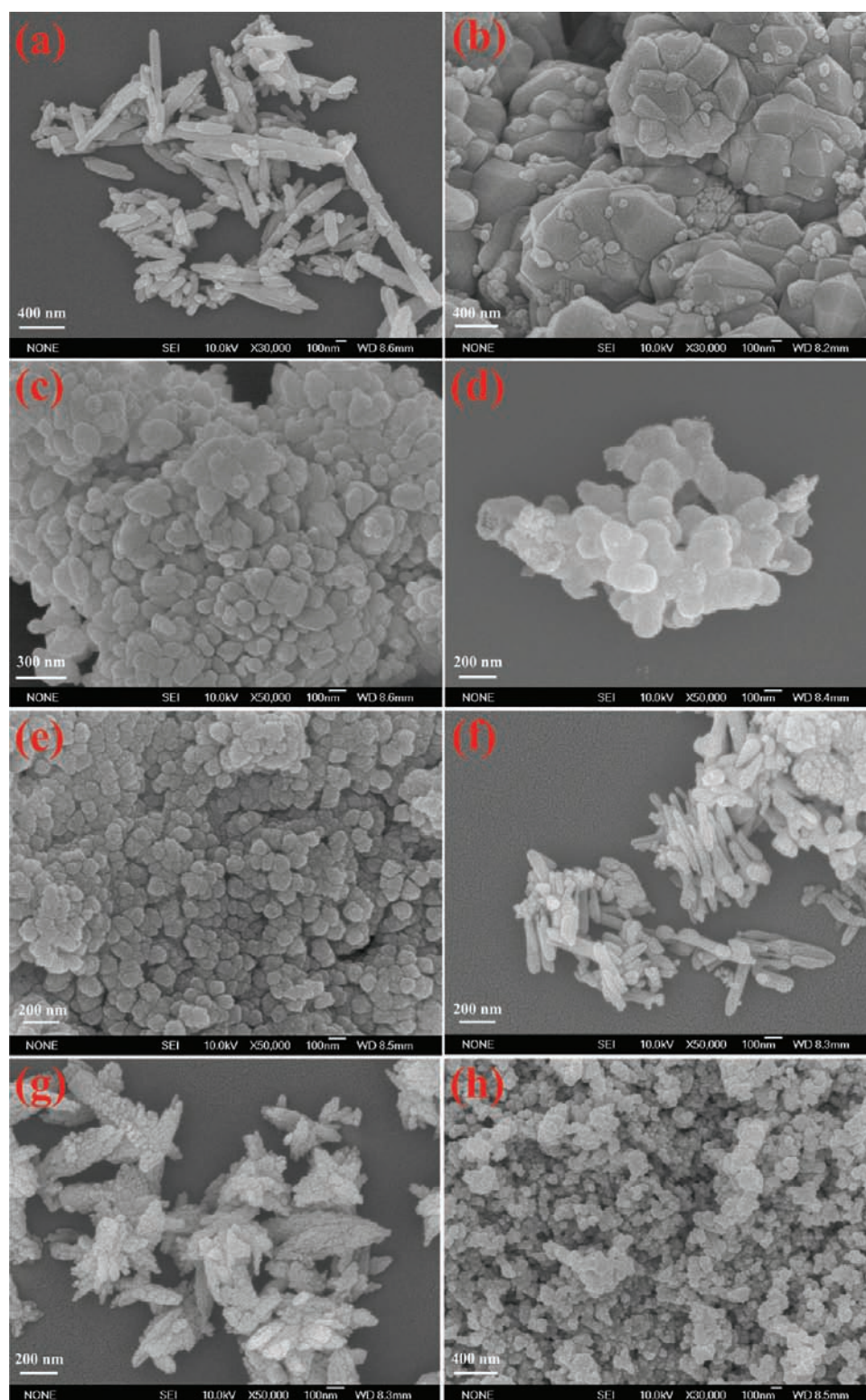


**Figure 2.** SEM images of the samples prepared in various solvents: (a) water ( $\text{H}_2\text{O}$ ), (b) benzene, (c) cyclohexane, (d) diethylene glycol dimethyl ether, (e) caprylcaldehyde, (f) acetone, (g) methanoic acid, and (h) ethylene glycol.

The differential thermal gravimetry (DTG) data indicate that this mass loss process underwent three steps, which have been fitted in Gaussian curves. The first process, as indicated by a Gaussian peak at  $134\text{ }^\circ\text{C}$  in Figure 5b, could be ascribed to the dehydration of adsorbed water. The second one represented by a Gaussian peak at  $217\text{ }^\circ\text{C}$  could be derived from the dehydration process of lattice water, as confirmed by the

presence of an endothermic peak at  $217\text{ }^\circ\text{C}$  in DTA curve. The last one, with a peak centered at  $230\text{ }^\circ\text{C}$ , is due to the decomposition of organics and carbonate absorptions from sample surfaces. From the integrated areas of these three Gaussian peaks, the amounts of water-derived species and surface organic species were calculated to be 3.23 and 1.27 wt %, respectively. Based on the Eu content determined by ICP

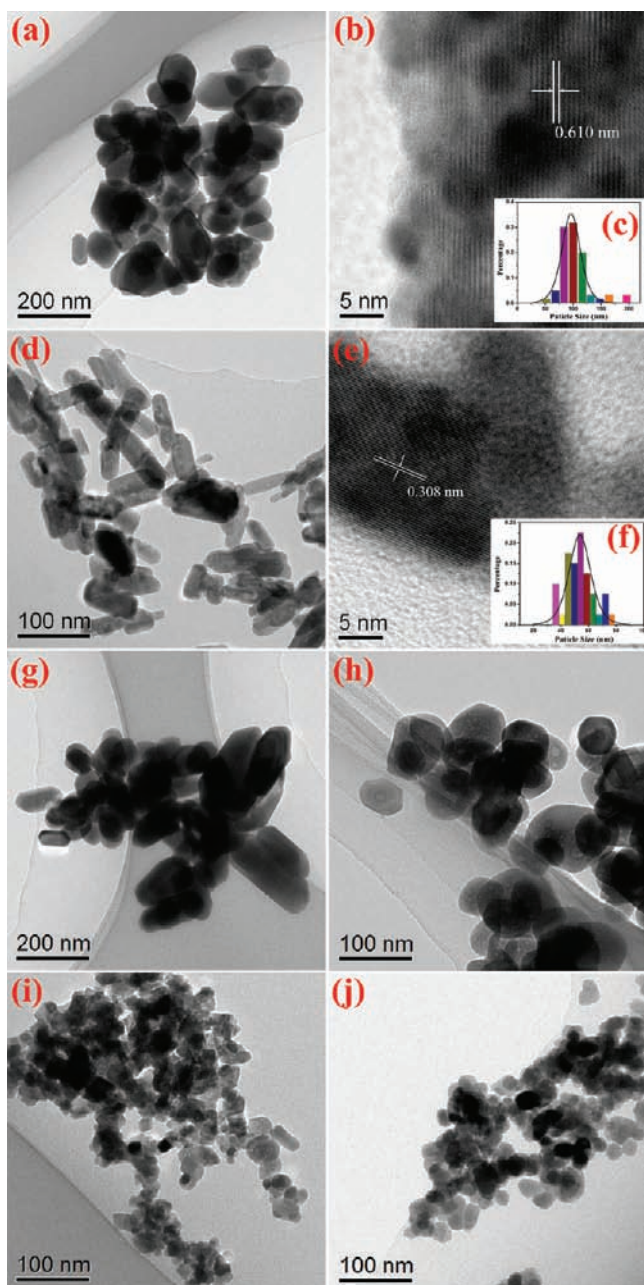


**Figure 3.** TEM and HRTEM images of  $\text{BiPO}_4:\text{Eu}^{3+}$  with different phases prepared in solvents: (a–c) benzene, (d–f) ethylene glycol, (g) tetranap, (h) directly milled, (i) propionic acid, and (j) ethylene glycol methyl ether.

(Table 1), the formula for sample S3 can be written as  $\text{Bi}_{0.969}\text{Eu}_{0.031}\text{PO}_4 \cdot 0.791\text{H}_2\text{O}$ . Similar TG curves were also observed for other samples. Following the same method, the water contents of all samples were determined and listed in Table 1. It is obvious that samples containing HP phase contained water molecules more than those samples in pure LTMP phase, although the latter ones have relatively smaller particle sizes. In addition, an exothermic peak in DTA curve was also detected at  $618^\circ\text{C}$  in Figure 5a, which could be due to the phase transformation from HP to LTMP, because of the absence of mass loss at this temperature.

**3.2. Photoluminescence Variations with Phase Tailoring.** Figure 6 compares the photoluminescence excitation and emission spectra of samples S3 and S11, prepared in benzene

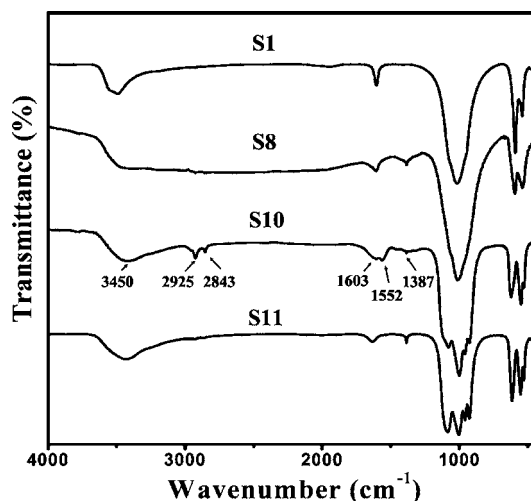


**Figure 4.** IR spectra of samples S1, S8, S10, and S11, prepared in solvents of water, acetone, methanoic acid, and ethylene glycol methyl ether, respectively.

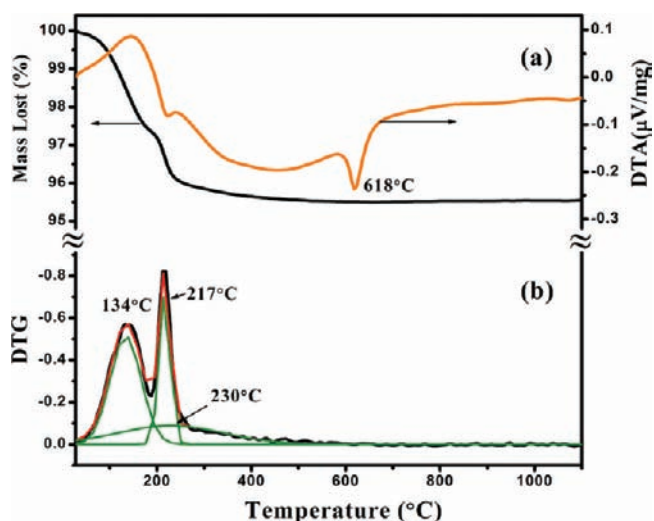


**Figure 5.** TG-DTA curves of sample S3 prepared in benzene solvent. Red line denotes the fitting curve of DTG.

and ethylene glycol methyl ether, respectively. The excitation spectra were determined by monitoring the emission of  ${}^5\text{D}_0\text{--}{}^7\text{F}_1$  at 593 nm. The broad band centered between 250 and 300 nm is ascribed to the charge-transfer band (CT band) that results from the transition of ligand  $\text{O}^{2-}$  2p orbital to the empty states of  $4f^6$  configuration of  $\text{Eu}^{3+}$  (i.e.,  $\text{Eu}^{3+}\text{--}\text{O}^{2-}$  transition). The peaks in the range from 300 to 410 nm are attributed to the direct excitation of  $\text{Eu}^{3+}$  ground state to higher levels of  $4f^6$ -manifold, including  ${}^7\text{F}_0\text{--}{}^5\text{H}_3$  (317 nm),  ${}^7\text{F}_0\text{--}{}^5\text{D}_4$  (361 nm),  ${}^7\text{F}_0\text{--}{}^5\text{L}_7$  (375, 381, 385 nm),  ${}^7\text{F}_0\text{--}{}^5\text{L}_6$  (394 nm).<sup>5,19</sup>

Emission spectra of samples S3 and S11 are attributed to luminescence spectrum of Eu ions.<sup>5,20,21</sup> The emission spectra were measured at room temperature by monitoring the excitation wavelength of  ${}^7\text{F}_0\text{--}{}^5\text{L}_6$  at 394 nm. It is seen that samples S3 and S11 showed similar emission lines but different intensities. Qian et al. concluded that phase type is not the main factor for the different emission intensities; instead, the morphology is the main factor.<sup>16</sup> The band centered at 593 nm with a weaker shoulder at 587 nm can be ascribed to  ${}^5\text{D}_0\text{--}{}^7\text{F}_1$  transition. The bands in the range of 610–622 nm and

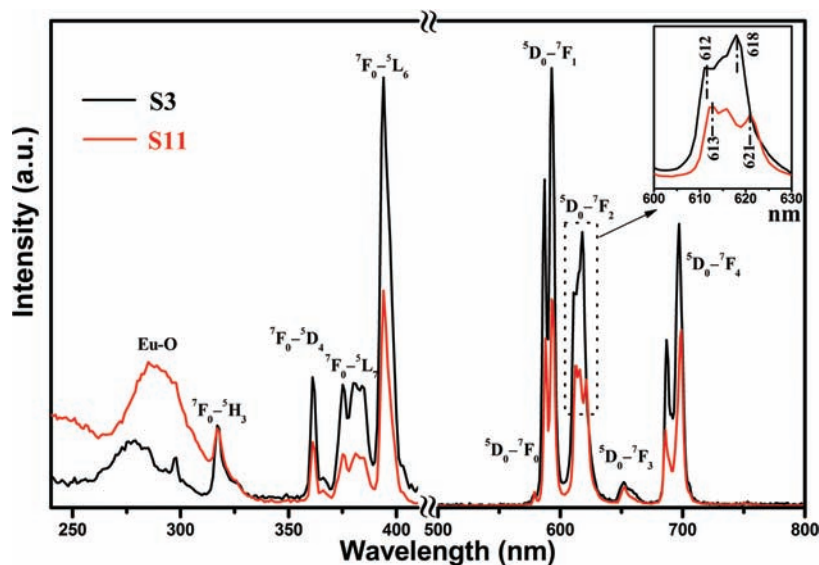


**Figure 6.** Excitation and emission spectra of sample S3 in HP and S11 in LTMP prepared in solvents of benzene and ethylene glycol methyl ether.

685–698 nm can be assigned to  ${}^5D_0-{}^7F_2$  and  ${}^5D_0-{}^7F_4$  transitions, respectively. The remained peaks at 578 and 652 nm could be stemmed from the transitions  ${}^5D_0-{}^7F_0$  and  ${}^5D_0-{}^7F_3$ , respectively.<sup>22,23</sup> Scaling up the bands in the range of 610–622 nm, one can see that the  ${}^5D_0-{}^7F_2$  peaks for samples S3 in HP and S11 in LTMP are quite different (see inset of Figure 6). Both peaks at 612 and 618 nm for sample S3 shifted toward higher wavelengths of 613 and 621 nm for sample S11, while the corresponding peak intensities became weakened. This observation is very difficult to be understood within the framework of crystal field theory, since (i) the  ${}^5D_0-{}^7F_2$  transition is an electronic dipole transition and hypersensitive to the crystal field environment; (ii) the symmetry of crystal fields around  $\text{Eu}^{3+}$  for LTMP phase is lower than that in the HP phase; and (iii) the lower symmetry of crystal fields usually gives rise to a more intensive emission, which is opposite to what was observed for samples S3 and S11. Instead, this difference in peak intensity could be closely related to the surface ligands and the relevant luminescence quenchers when using different solvents.

Luminescence decay curves monitored by  ${}^5D_0-{}^7F_1$  transition ( $\lambda_{\text{ex}} = 394$  nm) of  $\text{Eu}^{3+}$  for samples S3 and S11 are presented in Figure 7. For sample S3, the luminescence decay curve could be

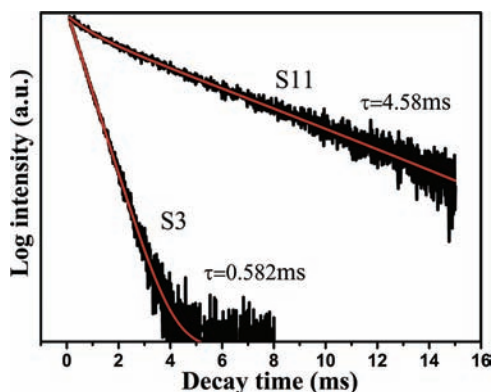


**Figure 7.** Decay time curves of sample S3 in HP and sample S11 in LTMP prepared in solvents benzene and ethylene glycol methyl ether, respectively. Red lines are the data-fit results for the decay time curves.

well-fitted using single exponential decay in terms of  $I = I_0 \exp(-t/\tau)$ , where  $\tau$  is the lifetime. The lifetime  $\tau$  is calculated to be 0.582 ms. Comparatively, for sample S11, a double exponential function can reproduce the decay curve well, namely,

$$I = A_1 \exp\left(\frac{-t}{\tau_1}\right) + A_2 \exp\left(\frac{-t}{\tau_2}\right)$$

where  $\tau_1$  and  $\tau_2$  are two different interval times, and  $A_1$  and  $A_2$  are the respective fitting parameters. The average lifetime is defined as  $\langle \tau \rangle = (A_1\tau_1^2 + A_2\tau_2^2)/(A_1\tau_1 + A_2\tau_2)$ .<sup>24,25</sup> For sample S11,  $\tau_1$  and  $\tau_2$  were 0.86 and 4.79 ms, respectively. As a result, the average lifetime is 4.58 ms.

On the basis of emission spectra and decay time, the quantum efficiency ( $\eta$ ) can be calculated in terms of  $\eta = A_{\text{rad}}/(A_{\text{rad}} + A_{\text{nrad}})$ ,<sup>26</sup> where both terms  $A_{\text{rad}}$  and  $A_{\text{nrad}}$  denote the radiative and nonradiative transition rates, respectively. The term  $A_{\text{rad}}$  can be collected using an integrate region and is defined as<sup>5</sup>

$$A_{\text{rad}} = \sum_{j=0}^4 A_{0j}$$

where  $A_{0j} = A_{01}(I_{0j}/I_{01})(\nu_{01}/\nu_{0j})$  and  $A_{01}$  is the Einstein's coefficient of spontaneous emission between the  ${}^5D_0$  and  ${}^7F_1$  levels, which is  $50 \text{ s}^{-1}$ . In addition,  $I_{0j}$  and  $\nu_{0j}$  denote the integrate proportion and energy core of emission band  ${}^5D_0-{}^7F_j$ , respectively. Moreover, the relationship among lifetime ( $\tau$ ), radiative ( $A_{\text{rad}}$ ), and nonradiative ( $A_{\text{nrad}}$ ) transition rates can be defined as<sup>27</sup>

$$\frac{1}{\tau} = A_{\text{rad}} + A_{\text{nrad}}$$

Finally, the quantum efficiency values ( $\eta$ ) can be obtained, which is 8.95% for sample S2 (HP) and 81.9% for sample S11 (LTMP), respectively. The average lifetime and quantum efficiency for all samples are compared in Figure 8 and Table 3. It can be seen that the samples in pure HP phase exhibited relatively shorter lifetime and lower quantum efficiency. With

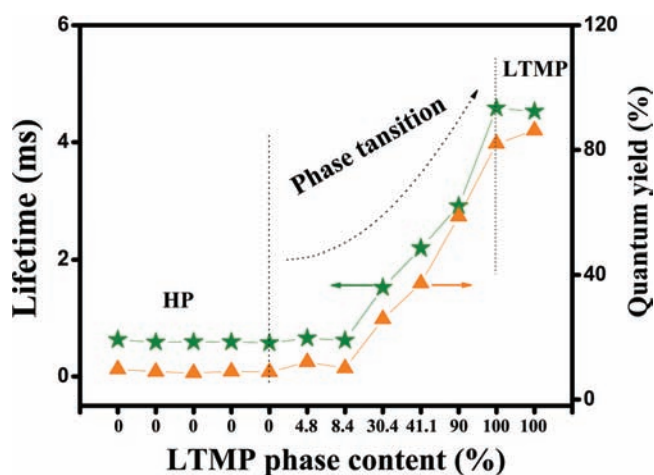


Figure 8. Illustration of variation tendency of lifetime and quantum yield for all samples with different phase content.

Table 3. Average Lifetime, Radiative Transition Rate ( $A_{\text{rad}}$ ), and Quantum Efficiency for All Samples

sample	lifetime (ms)	$A_{\text{rad}}$	quantum efficiency (%)
S1	0.629(1)	154.424	9.71(2)
S2	0.586(1)	152.809	8.95(2)
S3	0.582(1)	146.504	8.53(1)
S4	0.590(2)	152.042	8.97(3)
S5	0.575(1)	153.253	8.81(2)
S6	0.654(4)	184.600	12.07(7)
S7	0.616(2)	163.566	10.08(3)
S8	1.52(1)	169.733	25.8(2)
S9	2.19(1)	170.382	37.3(2)
S10	2.91(2)	201.584	58.6(4)
S11	4.58(3)	178.879	81.9(5)
S12	4.52(4)	190.550	86.2(8)

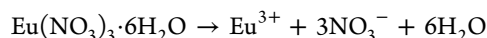
increasing the phase content of LTMP, the average lifetime and quantum efficiency showed an increasing trend.

## 4. DISCUSSION

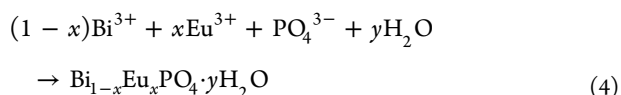
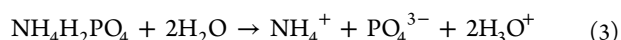
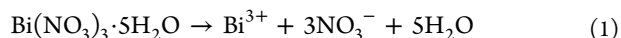
**4.1. Formation Mechanism of  $\text{BiPO}_4\cdot\text{Eu}^{3+}$  in Different Solvents.** To reveal the formation of HP and LTMP phases in different solvents, several factors, such as lattice water, types and properties of solvents, and properties of starting materials should be well-addressed. First, lattice water is a key factor for the formation of HP, because HP is a hydrated phase, while LTMP is not, and the water molecules favor the formation of hexagonal  $\text{BiPO}_4$ .<sup>4,28,29</sup> Second, depending on the chemical nature, solvents may have different function groups, and thus exhibit different properties. For instance, organic tetranap, benzene, and cyclohexane are hydrophobic, while other solvents are hydrophilic. Furthermore, chemicals such as  $\text{Bi}(\text{NO}_3)_3$ ,  $\text{Eu}(\text{NO}_3)_3$ , and  $\text{NH}_4\text{H}_2\text{PO}_4$  cannot be dissolved in tetranap, benzene, and cyclohexane, but slightly dissolved in other solvents except for ethylene glycol and ethylene glycol methyl ether. Third,  $\text{Bi}^{3+}$  ions are easily coordinated with P–O groups of  $\text{H}_2\text{PO}_4^-$ ,  $\text{H}_2\text{PO}_4^-$ , and  $\text{PO}_4^{3-}$  to form compounds in solution.<sup>10</sup> Based on these considerations, the possible mechanism for formation of HP and LTMP in different solvents could be discussed as follows.

**4.1.1. Formation of HP Phase in Water.** Only HP was formed, when water was used as the solvent. The reaction process can be described by eqs 1–4. First,  $\text{Eu}(\text{NO}_3)_3\cdot 6\text{H}_2\text{O}$

and  $\text{Bi}(\text{NO}_3)_3\cdot 5\text{H}_2\text{O}$  were dissolved in water to ionize  $\text{Bi}^{3+}$  and  $\text{Eu}^{3+}$  ions, which is followed by a hydrolysis reaction that occurs for  $\text{Bi}^{3+}$  ions to form  $\text{BiONO}_3$  precipitation and establishes a chemical equilibrium (eq 2).<sup>30–32</sup> When  $\text{NH}_4\text{H}_2\text{PO}_4$  was added, phosphate ion ( $\text{PO}_4^{3-}$ ) and hydronium ( $\text{H}_3\text{O}^+$ ) were produced, as described in eqs 3. Finally,  $\text{Bi}^{3+}$ ,  $\text{Eu}^{3+}$ ,  $\text{H}_2\text{O}$ , and  $\text{PO}_4^{3-}$  were combined to generate  $\text{Eu}^{3+}$ -doped HP. Once the concentration of  $\text{Bi}^{3+}$  in solution was decreased, the reaction 2 will go on until all  $\text{PO}_4^{3-}$  ions were consumed.



and



### 4.1.2. Formation of HP Phase in Hydrophobic Solvents.

Tetranap and benzene are aromatic compounds, while cyclohexane belongs to the cycloalkane series. As mentioned above, these solvents are hydrophobic, in which all starting materials, such as  $\text{Bi}(\text{NO}_3)_3\cdot 5\text{H}_2\text{O}$ ,  $\text{Eu}(\text{NO}_3)_3\cdot 6\text{H}_2\text{O}$ , and  $\text{NH}_4\text{H}_2\text{PO}_4$ , are not soluble. When the starting materials were mixed, they maintained the solid state. The crystallized water molecules from the starting materials can provide a local hydrated region, and thus the formation of HP was favored. This situation is similar to the solid-state reactions at room temperature, and the stirring procedure is similar to the grinding. Indeed, we obtained HP through direct milling of the starting materials at room temperature, as confirmed by XRD pattern (sample S5).

**4.1.3. Formation of LTMP and mixed phase in hydrophilic solvents. (1). Alcohols.** The LTMP phase was, for the first time, obtained at room temperature using alcohols, such as ethylene glycol methyl ether (EGME) and ethylene glycol (EG) as solvents. As is known to all, alcohols are a type of compounds that have a hydroxyl group (–OH) bonded to a saturated,  $\text{sp}^3$ -hybridized carbon atom.<sup>33</sup> Because of the strong polarity of the O–H bond, the O atom is easy to coordinate with other ions. The starting materials ( $\text{Bi}(\text{NO}_3)_3$  and  $\text{Eu}(\text{NO}_3)_3$ ) can be completely dissolved in EG and EGME. The relatively stable complexes ( $\text{Bi-EG}$ ,  $\text{Bi-EGME}$  complexes)<sup>34–36</sup> then would be formed, as shown in Figure 9.<sup>37</sup>

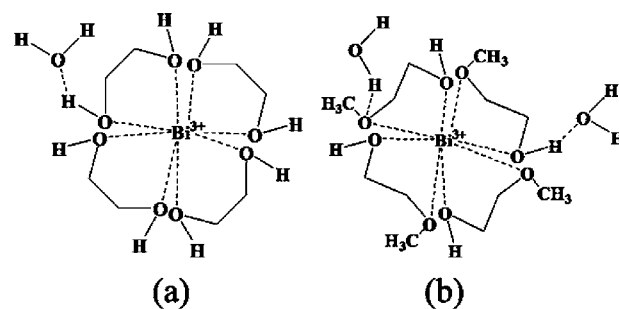


Figure 9. The existing forms of  $\text{Bi}^{3+}$  in alcoholic solvents: (a) ethylene glycol, and (b) ethylene glycol methyl ether.



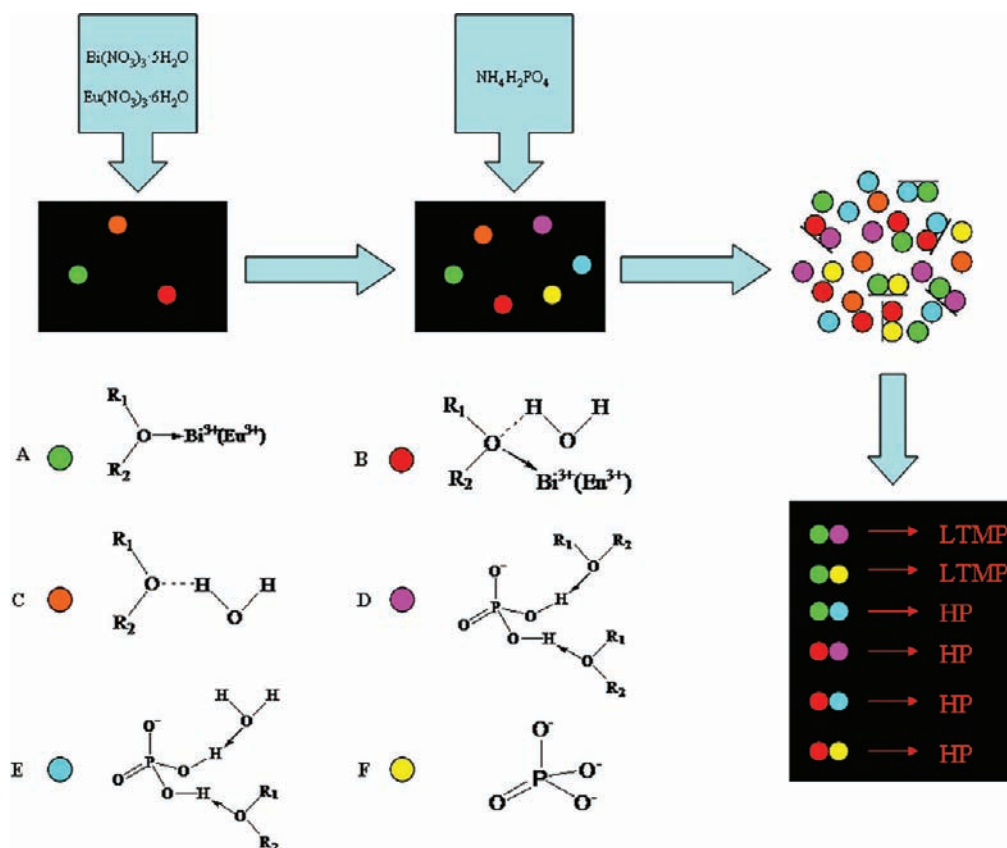


Figure 10. Illustration of formation mechanism of  $\text{BiPO}_4:\text{Eu}^{3+}$  in an etheric solvent.

Here,  $\text{Bi}^{3+}$  was encompassed by EG or EGME, possibly because  $\text{Bi}^{3+}$  ions adopt an eight-oxygen coordination structure in HP and LTMP.<sup>4</sup> In this way, the complexes would prevent the water molecules approaching to  $\text{Bi}^{3+}$ , and thus LTMP can be favorably formed when  $\text{NH}_4\text{H}_2\text{PO}_4$  was added. It is concluded that the presence of alcohol hydroxyl is in favor of the formation of LTMP. The formation mechanism of LTMP in alcohols was quite different from the previous reports (ref 34), in which the formation of LTMP was attributed to the high boiling point of EG.

(2). *Ethers*. Sample S6 prepared in diethylene glycol dimethyl ether ( $\text{CH}_3\text{OCH}_2\text{CH}_2\text{OCH}_2\text{CH}_2\text{OCH}_3$ ) crystallized in HP with a very small amount of LTMP, apparently different from sample S11 obtained in EGME ( $\text{HOCH}_2\text{CH}_2\text{OCH}_3$ ). The big difference is that the latter one contains an alcohol hydroxyl, while only ether groups are present for the former one.

Ethers were featured by C–O–C linkage with a bond angle of ca.  $104.5^\circ$  and a C–O distance of ca. 140 pm. The O atom is bonded to two C atoms of  $\text{sp}^3$  hybridization. Because of the existence of two lone electron pairs, the O atom can form hydrogen bonds with proton of water, and it can also form coordinate bonds with metal ions.<sup>33</sup> Compared to that of alcohol hydroxyl, oxygen atom of ether group has a relatively weaker polarity, which would lead to a weaker coordination with  $\text{Bi}^{3+}$  and  $\text{Eu}^{3+}$  ions were not surrounded by the O atom of an ether group such as EG. The formation of HP mixed with a small amount of LTMP in etheric solvents, taking diethylene glycol dimethyl ether as an example, is illustrated in Figure 10. Once  $\text{Bi}(\text{NO}_3)_3 \cdot 5\text{H}_2\text{O}$  and  $\text{Eu}(\text{NO}_3)_3 \cdot 6\text{H}_2\text{O}$  were added into etheric solvents, coordination complexes, and hydrogen bonds

would be formed, as shown by A, B, and C in Figure 10. The amount of B is the majority, far surpassing that of A, because the amount of water is  $\sim 5$  times larger than that of  $\text{Bi}^{3+}$  in the starting materials of  $\text{Bi}(\text{NO}_3)_3 \cdot 5\text{H}_2\text{O}$ . When  $\text{NH}_4\text{H}_2\text{PO}_4$  was added,  $\text{H}_2\text{PO}_4^-$  formed a hydrogen bond with the ether group (see Figure 10D). Subsequently,  $\text{H}_2\text{O}$  molecules from C can promote D to ionize another salt (E), and further to  $\text{PO}_4^{3-}$  (F). Only a small amount of  $\text{H}_2\text{PO}_4^-$  was ionized, because of the very low amount of  $\text{H}_2\text{O}$ . Comparatively, a large amount of  $\text{H}_2\text{PO}_4^-$  exists as D form while the number of E and F is only a little. For coordination complex B,  $\text{H}_2\text{O}$  molecules, which have two lone pair electrons in the O atom, are present near  $\text{Bi}^{3+}$  and  $\text{Eu}^{3+}$  ions. Therefore, the reactions between complexes such as A–E, B–E, B–D, and B–F, yield HP. Alternatively, the combination of A with D or F might form LTMP. Because of the low concentration of complexes A and F, the production rate of LTMP is slightly low. Therefore, in an etheric solvent, the formation of HP was dominant, just with a small amount of LTMP. Therefore, in an etheric solvent, the final product is a mixed phase of dominant HP and a small amount of LTMP. The presence of the C–O–C group is crucial for the formation of HP phase.

(3). *Aldehydes, Ketones, and Carboxylic Acids*. Because of the lack of hydroxyl functional groups, the samples prepared in caprylaldehyde and acetone should be only in HP. However, XRD analysis showed that the content of HP was only 91.6% obtained in caprylaldehyde. HP phase content decreased to 69.6% in acetone, and further 58.9% in propionic acid. While in methanoic acid, LTMP became a dominant phase (90%). These observations were closely related to the carbonyl group  $\text{C}=\text{O}$ . As is well demonstrated, caprylaldehyde, acetone,

propionic acid, and methanoic acid have the common carbonyl group  $\text{C}=\text{O}$ , but belong to three different types of organic compounds (i.e., aldehydes, ketones, and carboxylic acids, respectively). More importantly,  $\text{C}=\text{O}$  double bonds are polarized, because of the high electronegativity of oxygen, relative to carbon. Since the carbonyl carbon is positively polarized, it is electrophilic (a Lewis acid) and reacts with nucleophiles. Conversely, the carbonyl oxygen is negatively polarized and nucleophilic (a Lewis base). Moreover, the negative polarity (electron-rich,  $\delta^-$ ) of the O atom in carbonyl group decreases in the order of aldehydes, ketones, and carboxylic acids due to the inductive effect,<sup>33</sup> the same as the reducing order of HP content. This strongly implies that negative polarity of the O atom is crucial for the decrease of HP content.

The formation of mixed phase of HP and LTMP in aldehydes, ketones, and carboxylic acids was discussed first. When  $\text{Bi}(\text{NO}_3)_3 \cdot 5\text{H}_2\text{O}$  and  $\text{Eu}(\text{NO}_3)_3 \cdot 6\text{H}_2\text{O}$  were added to aldehydes, ketones, and carboxylic acids,  $\text{Bi}^{3+}$  and  $\text{Eu}^{3+}$  were attracted to the oxygen atom in carbonyl group. Subsequently,  $\text{H}_2\text{PO}_4^-$  was pulled into the C atom of the carbonyl group, and further partially ionized to  $\text{HPO}_4^{2-}$ ,  $\text{PO}_4^{3-}$ , and  $\text{H}_3\text{O}^+$ .  $\text{HPO}_4^{2-}$  and  $\text{PO}_4^{3-}$  were also attracted by the C atom in the carbonyl group, while  $\text{H}_3\text{O}^+$  was dragged by the O atom into the carbonyl group. A similar nuclei, as depicted in Figure 11, in

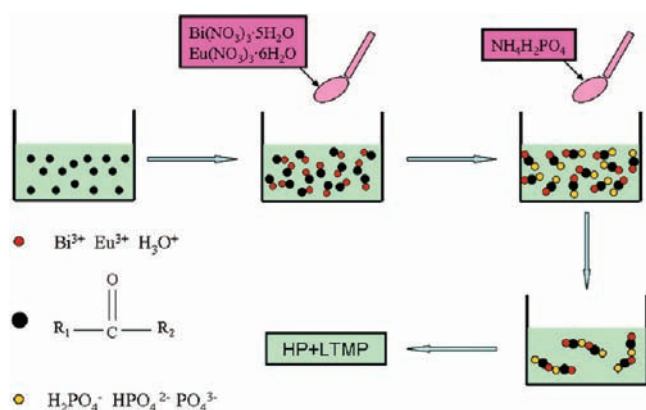


**Figure 11.** Illustration of formation process of  $\text{BiPO}_4:\text{Eu}^{3+}$  prepared in aldehydes, ketones, and carboxylic acids.

which  $\text{Bi}^{3+}$ ,  $\text{Eu}^{3+}$ , and  $\text{H}_3\text{O}^+$  were gathered at the vicinity of the O atom, while  $\text{H}_2\text{PO}_4^-$ ,  $\text{HPO}_4^{2-}$ , and  $\text{PO}_4^{3-}$  were at the vicinity of the C atom. Therefore, during the collision of solvent molecules,  $\text{Bi}^{3+}$  ions along with  $\text{H}_3\text{O}^+$  and  $\text{H}_2\text{PO}_4^-/\text{HPO}_4^{2-}/\text{PO}_4^{3-}$  ions would combine with each other to form HP. On the other hand, when  $\text{Bi}^{3+}$  directly reacted with  $\text{H}_2\text{PO}_4^-/\text{HPO}_4^{2-}/\text{PO}_4^{3-}$ , LTMP would be formed. Herein, a mixed phase of HP and LTMP could be expected in aldehydes, ketones, and carboxylic acids.

Furthermore, the relationship between the phase content of HP in caprylaldehide, acetone, propionic acid, and methanoic acid was also discussed. As analyzed above, the content of HP phase is determined by the concentration of  $\text{H}_3\text{O}^+$ , together with  $\text{Bi}^{3+}$  ions at the vicinity of the O atom in the carbonyl group. This concentration is dependent on the electron-rich ( $\delta^-$ ) component of the O atom in the carbonyl group. The more electron-rich ( $\delta^-$ ) O atom is, the more easily attached cations are in its vicinity. From aldehydes, ketones to carboxylic acids, the negative charge ( $\delta^-$ ) of the O atom in carbonyl group

decreases, which suggested that less  $\text{H}_3\text{O}^+$  and  $\text{Bi}^{3+}$  ions have the chance to be presented at the vicinity of the O atom. Therefore, the phase content of HP should show a decreasing trend from aldehydes, to ketones, and to carboxylic acids. In addition, using the carboxylic acid as a solvent, the existence of hydroxyl group can also promote the formation of LTMP, which is similar to the case in EG, as we discussed in Figure 8. Therefore, the LTMP phase became the dominate one in sample S10 obtained in methanoic acid.

#### 4.2. Phase-Related Particle Sizes of $\text{BiPO}_4:\text{Eu}^{3+}$ Nanocrystals for Solvent-Driven Room-Temperature Synthesis.

As listed in Table 2, the average particle sizes for the samples in HP were  $\sim 100$  nm, which is larger than that for samples in LTMP (50 nm). To understand this phase-related particle size behavior for  $\text{BiPO}_4:\text{Eu}^{3+}$  nanocrystals under solvent-driven room-temperature synthesis, it is necessary to pay attention to the crystallization process. Just like the formation of most nanoparticles, the crystallization process of  $\text{BiPO}_4:\text{Eu}^{3+}$  nanocrystals basically consisted of a nucleation step, followed by particle growth stages. In the solvent-driven synthesis of  $\text{BiPO}_4:\text{Eu}^{3+}$  polymorphs at room temperature, the nucleation is the step where  $\text{Bi}^{3+}$  and  $\text{Eu}^{3+}$  in the solvents reacted with  $\text{PO}_4^{3-}$  to get together in forming clusters at the nanometer scale. These clusters need to reach a critical size in order to become the stable nuclei. Subsequently, the reactant ions (monomers) in the solution would react each other at the surfaces of nucleus to make the crystal of  $\text{BiPO}_4:\text{Eu}^{3+}$  grow. As is well-known, high monomer concentration at the surface of nuclei favors the growth of particles. The monomer concentration remained in the reaction solution can be depleted by the nucleation and growth of the nanocrystals.<sup>38–40</sup>

In a water solvent, as indicated by eq 2, hydrolysis of  $\text{Bi}(\text{NO}_3)_3$  results in a barely soluble  $\text{BiONO}_3$ . The lower concentration of  $\text{Bi}^{3+}$  in the solution gives rise to a smaller amount of HP phase nucleus, because of the reaction of eq 4. The formation of  $\text{BiPO}_4:\text{Eu}^{3+}$  nucleus leads to a decrease in the concentration of  $\text{Bi}^{3+}$  ions in the solution, and the reaction of eq 2 goes on conversely to keep the balance of dissolution. The newly ionized  $\text{Bi}^{3+}$  ions would diffuse in the solution and react with  $\text{PO}_4^{3-}$  and  $\text{H}_3\text{O}^+$  on the surfaces of  $\text{BiPO}_4:\text{Eu}^{3+}$  nucleus. The water solvent has a lower viscosity, which may promote the motion of monomers to give a higher monomer concentration at the surfaces of nuclei, which would lead to a fast growth rate and large particle size.<sup>34</sup> In hydrophobic solvents such as tetranap, benzene, and cyclohexane, such a situation is maintained as in water.

In an alcohol solvent,  $\text{BiPO}_4:\text{Eu}^{3+}$  crystallized in a monoclinic structure with a relatively small particle size. As is known, LTMP is a thermodynamically stable phase, while HP is metastable.<sup>4</sup> The different thermodynamic stabilities of HP and LTMP affect their nucleation rate, because the energy for nucleation of HP is higher than that of LTMP. Therefore, it can be expected that the concentration of nucleation for LTMP is much higher than that for HP. A larger number of LTMP nucleation reduced the monomer concentration on the surface of nuclei, which results in a lower growth rate and a relatively small particle size.

In solvents of ethers, aldehydes, ketones, and carboxylic acids, a mixed phase of HP and LTMP was obtained, in which the particle size for HP component was larger than that for LTMP. As discussed above, water is a key for formation of HP structure. The lower concentration of water in reaction solution resulted in a lower number of nucleation of HP. On the other

hand, existence of water around HP nucleus reduces the viscosity of solution and improves the diffusion of monomer. Therefore, the HP component has a relatively larger particle size, in comparison to the LTMP component in the samples of mixed phases.

In order to further confirm the unique crystal growth behavior, a series of time-dependent experiments were performed. Figure 12 shows the TEM images of the samples

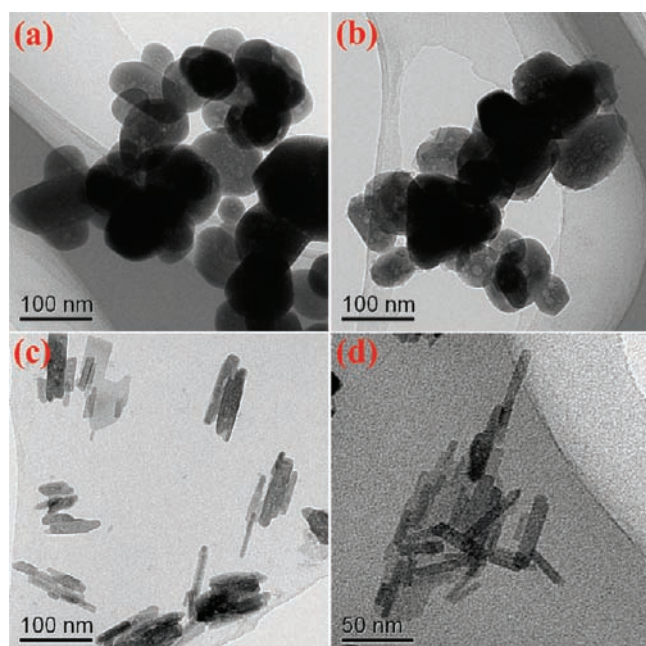


**Figure 12.** TEM images of the samples prepared in solvent benzene for different periods of reaction time: (a) 1 h and (b) 2 h. TEM images of the samples prepared within 2 h in solvent EG for different periods of reaction time: (c) 1 h and (d) 2 h.

obtained in solvents of benzene and EG after reactions for 1 and 2 h, respectively. When the reactions were carried out for 1 and 2 h, the particle sizes of the samples in HP prepared in a benzene solvent were bigger than those in LTMP prepared in solvent EG. This means that HP has a faster growth rate than LTMP.

## 5. CONCLUSION

$\text{BiPO}_4:\text{Eu}^{3+}$  nanocrystals were first prepared via a room-temperature precipitation method, using 11 solvents. The main results can be summarized as follows:

(i) The phase structure of  $\text{BiPO}_4:\text{Eu}^{3+}$  nanocrystals prepared at room temperature was highly dependent on the properties and function groups of solvents. Similar to that in water, hydrophobic organic solvents including tetrahydrofuran, benzene, and cyclohexane could promote the formation of hexagonal  $\text{BiPO}_4:\text{Eu}^{3+}$ , because of the local hydrated region provided by crystallized water molecules from the starting materials. In hydrophilic alcohols that contain only a hydroxyl group, a low-temperature monoclinic phase (LTMP) was steadily obtained. In other hydrophilic organic solvents, a mixed phase of hexagonal and low-temperature monoclinic  $\text{BiPO}_4:\text{Eu}^{3+}$  was formed because of the presence of C–O–C and C=O groups.

(ii) Particle sizes of  $\text{BiPO}_4:\text{Eu}^{3+}$  nanocrystals were closely related to the phase structures.  $\text{BiPO}_4:\text{Eu}^{3+}$  nanocrystals in a single-phase hexagonal structure exhibited a relatively larger

particle size. For example, the particle size of the nanocrystals prepared in benzene is on the order of one hundred (100) nanometers, which is much larger than that for the monoclinic structure.

(iii) The solvent has a great amount of influence on the Eu content in  $\text{BiPO}_4$  nanocrystals. Nanocrystals prepared in methanoic acid had a maximum Eu content, while that in ethylene glycol gave a minimum one. The photoluminescence spectra revealed that monoclinic  $\text{BiPO}_4:\text{Eu}^{3+}$  nanocrystals exhibited a longer lifetime and higher quantum yield than those for hexagonal structure.

## AUTHOR INFORMATION

### Corresponding Author

\*E-mail: lipingli@fjirsm.ac.cn.

### Notes

The authors declare no competing financial interest.

## ACKNOWLEDGMENTS

This work was financially supported by NSFC (Nos. 21025104, 51072198, 50972143, 91022018), National Basic Research Program of China (No. 2011CBA00501), and FJIRSM fund (No. 2010KL002). The authors express their thanks to Xiuqi Li from Brigham Young University for her valuable reading and comments.

## REFERENCES

- (1) Weissbuch, I.; Torbeev, V. Y.; Leiserowitz, L.; Lahav, M. *Angew. Chem., Int. Ed.* **2005**, *44*, 3226–3229.
- (2) Wang, F.; Han, Y.; Lim, C. S.; Lu, Y.; Wang, J.; Xu, J.; Chen, H.; Zhang, C.; Hong, M.; Liu, X. *Nature* **2010**, *463*, 1061–1065.
- (3) Zhang, J.; Ohara, S.; Umetsu, M.; Naka, T.; Hatakeyama, Y.; Adschiri, T. *Adv. Mater.* **2007**, *19*, 203–206.
- (4) Romero, B.; Bruque, S.; Aranda, M. A. G.; Iglesias, J. E. *Inorg. Chem.* **1994**, *33*, 1869–1874.
- (5) Zhao, M.; Li, G.; Zheng, J.; Li, L.; Wang, H.; Yang, L. *CrystEngComm* **2011**, *13*, 6251–6257.
- (6) Ruwet, M.; Ceckiewicz, S.; Delmon, B. *Ind. Eng. Chem. Res.* **1987**, *26*, 1981–1983.
- (7) Grabner, E. W.; Vermes, I.; König, K.-H. *J. Electroanal. Chem.* **1986**, *214*, 135–140.
- (8) Hölgye, Z. *J. Radioanal. Nucl. Chem.* **1998**, *227*, 127–128.
- (9) Pan, C.; Zhu, Y. *Environ. Sci. Technol.* **2010**, *44*, 5570–5574.
- (10) Guan, M.; Sun, J.; Tao, F.; Xu, Z. *Cryst. Growth Des.* **2008**, *8*, 2694–2697.
- (11) Liu, X.; Tian, B.; Yu, C.; Gao, F.; Xie, S.; Tu, B.; Che, R.; Peng, L.-M.; Zhao, D. *Angew. Chem., Int. Ed.* **2002**, *41*, 3876–3878.
- (12) Wang, H.; Li, G.; Guan, X.; Li, L. *J. Alloys Compd.* **2011**, *509*, 4160–4166.
- (13) Luwang, M. N.; Ningthoujam, R. S.; Srivastava, S. K.; Vatsa, R. K. *J. Am. Chem. Soc.* **2011**, *133*, 2998–3004.
- (14) Li, C.; Hou, Z.; Zhang, C.; Yang, P.; Li, G.; Xu, Z.; Fan, Y.; Lin, J. *Chem. Mater.* **2009**, *21*, 4598–4607.
- (15) Li, G.; Li, L.; Boerio-Goates, J.; Woodfield, B. F. *J. Am. Chem. Soc.* **2005**, *127*, 8659–8666.
- (16) Xue, F.; Li, H.; Zhu, Y.; Xiong, S.; Zhang, X.; Wang, T.; Liang, X.; Qian, Y. *J. Solid State Chem.* **2009**, *182*, 1396–1400.
- (17) Pokrovski, K.; Jung, K. T.; Bell, A. T. *Langmuir* **2001**, *17*, 4297–4303.
- (18) Wang, H.; Li, G.; Xue, Y.; Li, L. *J. Solid State Chem.* **2007**, *180*, 2790–2797.
- (19) Yaiphaba, N.; Ningthoujam, R. S.; Singh, N. S.; Vatsa, R. K.; Singh, N. R.; Dhara, S.; Misra, N. L.; Tewari, R. *J. Appl. Phys.* **2010**, *107*, 034301–9.
- (20) Xu, Z.; Kang, X.; Li, C.; Hou, Z.; Zhang, C.; Yang, D.; Li, G.; Lin, J. *Inorg. Chem.* **2010**, *49*, 6706–6715.

- (21) Xu, Z.; Cao, Y.; Li, C.; Ma, P. a.; Zhai, X.; Huang, S.; Kang, X.; Shang, M.; Yang, D.; Dai, Y.; Lin, J. *J. Mater. Chem.* **2011**, *21*, 3686–3694.
- (22) Phaomei, G.; Ningthoujam, R. S.; Singh, W. R.; Singh, N. S.; Luwang, M. N.; Tewari, R.; Vatsa, R. K. *Opt. Mater.* **2010**, *32*, 616–622.
- (23) Li, L. P.; Zhao, M. L.; Tong, W. M.; Guan, X. F.; Li, G. S.; Yang, L. S. *Nanotechnology* **2010**, *21*, 195601.
- (24) Su, Y.; Li, L.; Li, G. *Chem. Mater.* **2008**, *20*, 6060–6067.
- (25) Su, Y.; Li, L.; Li, G.; Liu, J.; Chen, X.; Hu, W.; Liu, G. *J. Nanosci. Nanotechnol.* **2010**, *10*, 1877–1883.
- (26) Su, Y.; Li, L.; Li, G. *J. Mater. Chem.* **2009**, *19*, 2316–2322.
- (27) Peng, C.; Zhang, H.; Yu, J.; Meng, Q.; Fu, L.; Li, H.; Sun, L.; Guo, X. *J. Phys. Chem. B* **2005**, *109*, 15278–15287.
- (28) Zhang, L.; Yin, M.; You, H.; Yang, M.; Song, Y.; Huang, Y. *Inorg. Chem.* **2011**, *50*, 10608–10613.
- (29) Arunkumar, P.; Jayajothi, C.; Jeyakumar, D.; Lakshminarasimhan, N. *RSC Adv.* **2012**, *2*, 1477.
- (30) Zhou, L.; Wang, W.; Xu, H.; Sun, S.; Shang, M. *Chem.—Eur. J.* **2009**, *15*, 1776–1782.
- (31) Yu, Y.; Jin, C. H.; Wang, R. H.; Chen, Q.; Peng, L. M. *J. Phys. Chem. B* **2005**, *109*, 18772–18776.
- (32) Kudo, A.; Omori, K.; Kato, H. *J. Am. Chem. Soc.* **1999**, *121*, 11459–11467.
- (33) McMurry, J. *Fundamentals of Organic Chemistry*, 5th Edition; Thomson—Brooks/Cole Publishing Company: Pacific Grove, CA, 2003.
- (34) Li, G.; Ding, Y.; Zhang, Y.; Lu, Z.; Sun, H.; Chen, R. *J. Colloid Interface Sci.* **2011**, *363*, 497–503.
- (35) Liu, Z.; Peng, S.; Xie, Q.; Hu, Z.; Yang, Y.; Zhang, S.; Qian, Y. *Adv. Mater.* **2003**, *15*, 936–940.
- (36) Gao, Y.; Niu, H.; Zeng, C.; Chen, Q. *Chem. Phys. Lett.* **2003**, *367*, 141–144.
- (37) Liang, X.; Kuang, S.; Li, Y. *J. Mater. Res.* **2011**, *26*, 1168–1173.
- (38) Burda, C.; Chen, X.; Narayanan, R.; El-Sayed, M. A. *Chem. Rev.* **2005**, *105*, 1025–1102.
- (39) Peng, Z. A.; Peng, X. *J. Am. Chem. Soc.* **2001**, *123*, 1389–1395.
- (40) Peng, Z. A.; Peng, X. *J. Am. Chem. Soc.* **2002**, *124*, 3343–3353.